Supporting Information

Macromolecular [2]Rotaxanes Linked with Polystyrene: Nanoscale Film Morphology and Properties

Brian J. Ree,[†,a] Daisuke Aoki,[†,b] Jehan Kim,[c] Toshifumi Satoh,[*,d] Toshikazu Takata,[*,b] and Moonhor Ree[*,c,e]

[a] Graduate School of Chemical Sciences and Engineering, Hokkaido University, Sapporo 060-8628, Japan
[b] Department of Chemical Science and Engineering, School of Materials and Chemical Technology, Tokyo Institute of Technology, 2-12-1 (H-126), Ookayama, Meguro-ku, Tokyo 152-8552, Japan
[c] Pohang Accelerator Laboratory, Pohang University of Science and Technology, Pohang 37673, Republic of Korea
[d] Faculty of Engineering, Hokkaido University, Sapporo 060-8628, Japan
[e] Department of Chemistry, Division of Advanced Materials Science, Pohang University of Science and Technology, Pohang 37673, Republic of Korea

Grazing Incidence X-Ray Scattering (GIXS) Data Analysis

The intensity of GIXS (I_{GIXS}) from structures in a thin film can be expressed by the scattering formula derived recently:[1-4]

$$I_{\mathrm{GIXS}}(\alpha_{\mathrm{f}},2\theta_{\mathrm{f}}) \cong \frac{1}{16\pi^2}\cdot\frac{1-e^{-2\,\mathrm{Im}(q_z)t}}{2\,\mathrm{Im}(q_z)}\cdot\begin{bmatrix} |T_{\mathrm{i}}T_{\mathrm{f}}|^2 I_1(q_{\|},\mathrm{Re}(q_{1,z})) + \\ |T_{\mathrm{i}}R_{\mathrm{f}}|^2 I_1(q_{\|},\mathrm{Re}(q_{2,z})) + \\ |T_{\mathrm{f}}R_{\mathrm{i}}|^2 I_1(q_{\|},\mathrm{Re}(q_{3,z})) + \\ |R_{\mathrm{i}}R_{\mathrm{f}}|^2 I_1(q_{\|},\mathrm{Re}(q_{4,z})) \end{bmatrix} \quad (1)$$

where α_f and $2\theta_f$ are the out-of-plane and in-plane exit angle of the out-going X-ray beam respectively, Im(q_z) = |Im($k_{z,f}$)| + |Im($k_{z,i}$)|, Re(x) is the real part of x, t is the film thickness, R_i and T_i are the reflected and transmitted amplitudes of the incoming X-ray beam respectively, and R_f and T_f are the reflected and transmitted amplitudes of the outgoing X-ray beam respectively. In addition, $q_{||} = \sqrt{q_x^2 + q_y^2}$, $q_{1,z} = k_{z,f} - k_{z,i}$, $q_{2,z} = -k_{z,f} - k_{z,i}$, $q_{3,z} = k_{z,f} + k_{z,i}$, and $q_{4,z} = -k_{z,f} + k_{z,i}$; here, $k_{z,i}$ is the z-component of the wave vector of the incoming X-ray beam, which is given by $k_{z,i} = k_o\sqrt{n_R^2 - \cos^2\alpha_i}$, and $k_{z,f}$ is the z-component of the wave vector of the outgoing X-ray beam, which is given by $k_{z,f} = k_o\sqrt{n_R^2 - \cos^2\alpha_f}$, where $k_o = 2\pi/\lambda$, λ is the wavelength of the X-ray beam, n_R is the refractive index of the film given by $n_R = 1 - \delta + i\zeta$ with dispersion δ and absorption ζ, and α_i is the out-of-plane grazing incident angle of the incoming X-ray beam. q_x, q_y, and q_z are the components of the scattering vector **q**. I_1 is the scattering intensity of the structure in the film, which can be calculated kinematically.

In eq 1, I_1 is the scattered intensity from morphological structures in the film and, thus, can be expressed by the following equation:[1-6]

$$I_1(\mathbf{q}) = P(\mathbf{q}) \cdot S(\mathbf{q}) \tag{2}$$

where $P(\mathbf{q})$ is the form factor that describes the shape, size, and orientation of scatterers in a thin film, and $S(\mathbf{q})$ is the structure factor which provides information on the relative positions of the group of scatterers, such as the crystal lattice parameters, orientation, dimension, and symmetry in an ordered structure and the interdistance of domains.

The measured GIXS (i.e., GISAXS) patterns inform that lamellar structures were formed in nanoscale films of PVL-*b*-PS, PVL-*rot*-PS-F and PVL-*rot*-PS-M. To analyze the GISAXS data, those lamellar structures may be appropriately handled by using a three layer model that is composed of a dense layer, a less dense layer, and their interfacial layer (Figure S15). For the lamellar structure consisted of three layers, the form factor $P(\mathbf{q})$ can be expressed by the following equation:

$$P(\mathbf{q}) = \left[\begin{array}{l} 4L_xL_yH_{inner}(\rho_{inner} - \rho_{outer}) \cdot \dfrac{\sin(q_xL_x)}{q_xL_x} \cdot \dfrac{\sin(q_yL_y)}{q_yL_y} \cdot \dfrac{\sin(q_zH_{inner})}{q_zH_{inner}} \; + \\ 4L_xL_yH_{outer}(\rho_{outer} - \rho_{matrix}) \cdot \dfrac{\sin(q_xL_x)}{q_xL_x} \cdot \dfrac{\sin(q_yL_y)}{q_yL_y} \cdot \dfrac{\sin(q_zH_{outer})}{q_zH_{outer}} \end{array} \right]^2 \quad (3)$$

where L_x and L_y are the length and width of lamellar structure respectively, H_{inner} and H_{outer} are the inner and outer layer heights respectively, and ρ_{inner} and ρ_{outer} are the relative electron densities of the inner and outer layers respectively. ρ_{matrix} is the relative electron density of the matrix layer. For the lamellar structure, H_{inner} corresponds to the crystal layer thickness (= d_{PVL}) having a relatively electron density ρ_{inner} (= ρ_{PVL}). The interfacial layer thickness (= d_i) having a relatively electron density ρ_{outer} (= ρ_i) is estimated from H_{inner} and H_{outer}: $d_i = (H_{outer} - H_{inner})/2$. The amorphous PS layer thickness d_{PS} having the relatively electron density ρ_{matrix} (= ρ_{PS}) is obtained from the long period D_L that is extracted from the structure factor $S(\mathbf{q})$: $d_{PS} = (D_L - d_{PVL} - 2d_i)$.

For the form factor, all structural parameters are further assumed to follow a Gaussian distribution $G(A)$:

$$G(A) = \frac{1}{\sqrt{2\pi}\sigma_A} \exp\left[-\frac{(A - \overline{A})^2}{2{\sigma_A}^2} \right] \quad (4)$$

where A can be one of the parameters, $\overline{A}$ is the mean value, and σ_A is the standard deviation of A from $\overline{A}$.

For a paracrystalline lattice consisting of the three layers described above, the structure factor $S(\mathbf{q})$ (the so-called interference function or lattice factor) can be determined from the Fourier transform of a complete set of lattice points.[1-4,7,8] In a paracrystal with distortion of the second kind, the positions of the lattice points can only be described with a positional distribution function (i.e., g-factor). In the simple case where the autocorrelation function of the crystal lattice is given by the convolution product of the distributions of the lattice points along three axes, and the distribution function is a Gaussian, $S(\mathbf{q})$ can be expressed by the following equation:[7]

$$S(\mathbf{q}) = \prod_{k=1}^{3} Z_k(\mathbf{q}) \tag{5}$$

$$Z_k(\mathbf{q}) = 1 + \frac{F_k(\mathbf{q})}{1 - F_k(\mathbf{q})} + \frac{F_k^*(\mathbf{q})}{1 - F_k^*(\mathbf{q})} \tag{6}$$

$$F_k(\mathbf{q}) = \left|F_k(\mathbf{q})\right| e^{-i\mathbf{q}\cdot\mathbf{a}_k} \tag{7}$$

$$\left|F_k(\mathbf{q})\right| = \exp\left[-\frac{1}{2}(q_1^2 g_1^2 + q_2^2 g_2^2 + q_3^2 g_3^2)\right]. \tag{8}$$

Here g_1, g_2, and g_3 (= g) are the components of the g-factor defined as

$$g_1 = \Delta\mathbf{a_1}/\mathbf{a_1} \tag{9a}$$

$$g_2 = \Delta\mathbf{a_2}/\mathbf{a_2} \tag{9b}$$

$$g_3 = \Delta\mathbf{a_3}/\mathbf{a_3} \tag{9c}$$

where $\mathbf{a_k}$ is the component of the fundamental vector $\mathbf{a}$ of the domain structure and $\Delta\mathbf{a_k}$ is the displacement of the vector $\mathbf{a_k}$. And q_1, q_2, and q_3 are the components of the scattering vector $\mathbf{q}$.

For the lamellar structure composed of three layers (Figure S15), the components of $\mathbf{q}$ in Equation 8 are defined by

$$q_1 = \mathbf{a_1}\cdot\mathbf{q_x} = |d_x \times \mathbf{q_x}| \tag{10a}$$

$$q_2 = \mathbf{a_2}\cdot\mathbf{q_y} = |d_y \times \mathbf{q_y}| \tag{10b}$$

$$q_3 = \mathbf{a_3}\cdot\mathbf{q_z} = |L \times \mathbf{q_z}| \tag{10c}$$

where d_x and d_y are the lattice dimension parameters (i.e., d-spacing values) along the q_x- and q_y-direction respectively, and L is the long period along the q_z-direction.

Moreover, for a structure with a given orientation in a film, its fundamental vectors can be rotated and transformed by a rotation matrix. When the structure of the film is randomly oriented in the plane of the film but uniaxially oriented out of plane, the peak position vector $\mathbf{q_c}$ of a certain reciprocal lattice point $\mathbf{c}^*$ in the sample reciprocal lattice is given by

$$\begin{aligned}\mathbf{q_c} &= \mathbf{R}\cdot\mathbf{c}^* \\ &\equiv (q_{c,x}, q_{c,y}, q_{c,z})\end{aligned} \tag{11}$$

where **R** is a 3 × 3 matrix to decide the preferred orientation of the structure in the film, and $q_{c,x}$, $q_{c,y}$, and $q_{c,z}$ are the x, y, z components of the peak position vector $\mathbf{q_c}$, respectively. Using Equation 11, every peak position can be obtained. Because of cylindrical symmetry, the Debye-Scherrer ring composed of the in-plane randomly oriented $\mathbf{c}^*$ cuts an Ewald sphere at two positions in its top hemisphere: $q_{\|} = q_{c,\|} \equiv \pm\sqrt{q_{c,x}^2 + q_{c,y}^2}$ with $q_z = q_{c,z}$. Thus diffraction patterns with cylindrical symmetry are easily calculated in the **q**-space. It is then convenient to determine the preferred orientation of known structures and further to analyze anisotropic X-ray scattering patterns. However, since **q**-space is distorted in GIXS by refraction and reflection effects, the relation between the detector plane expressed as the Cartesian coordinate defined by two perpendicular axes (i.e., by $2\theta_f$ and α_f) and the reciprocal lattice points is needed. The two wave vectors $k_{z,i}$ and $k_{z,f}$ are corrected for refraction as $k_{z,i} = k_o\sqrt{n_R^2 - \cos^2\alpha_i}$ and $k_{z,f} = k_o\sqrt{n_R^2 - \cos^2\alpha_f}$ respectively. Therefore, the two sets of diffractions that result from the incoming and outgoing X-ray beams, and denoted by q_1 and q_3 respectively, are given at the exit angles by the following expression:

$$\alpha_f = \arccos\left(\sqrt{n_R^2 - \left(\frac{q_{c,z}}{k_o} \pm \sqrt{n_R^2 - \cos^2\alpha_i}\right)^2}\right) \tag{12}$$

where $q_{c,z}/k_o > \sqrt{n_R^2 - \cos^2\alpha_i}$. In Equation 12, the positive sign denotes diffractions produced by the outgoing X-ray beam, and the negative sign denotes diffractions produced by the incoming X-ray beam. The in-plane incidence angle $2\theta_i$ is usually zero, so the in-plane exit angle $2\theta_f$ can be expressed as follow:

$$2\theta_{\mathrm{f}} = \arccos\left[\frac{\cos^2\alpha_{\mathrm{i}} + \cos^2\alpha_{\mathrm{f}} - \left(\frac{q_{\mathrm{c},||}}{\mathrm{k_o}}\right)^2}{2\cos\alpha_{\mathrm{i}}\cos\alpha_{\mathrm{f}}}\right]. \quad (13)$$

Therefore, diffraction spots detected on the detector plane in GIXS measurements can be directly compared to those derived using Equations 11-13 from an appropriate model and thus analyzed in terms of the model.

To obtain information on the orientation of the paracrystal lattice of the phase separated micro domain structures from GIXS data, the distribution of the orientation vector ***n*** is given by a function $D(\varphi)$, where φ is the polar angle between the ***n*** vector and the out-of-plane of the film (see an example in Figure S15); for example, φ is zero when the ***n*** vector in the film is oriented normal to the film plane. To calculate the 2D GIXS patterns, $D(\varphi)$ should be represented by a numerical function. In relation to the distribution of the lattice orientation, $D(\varphi)$ can generally be considered as a Gaussian distribution:

$$D(\varphi) = \frac{1}{\sqrt{2\pi}\sigma_\varphi}\exp\left[-\frac{(\varphi-\bar{\varphi})^2}{2\sigma_\varphi^2}\right] \quad (14)$$

where $\bar{\varphi}$ and σ_φ are the mean angle and standard deviation of φ from $\bar{\varphi}$, respectively. The observed scattering intensity $I_{\mathrm{GIXS},\varphi}(\mathbf{q})$ is obtained by integrating $I_{\mathrm{GIXS}}(\mathbf{q})$ over possible orientations of the lattice:

$$I_{\mathrm{GIXS},\varphi}(\mathbf{q}) = \int_{-\pi}^{\pi} I_{\mathrm{GIXS}}(\mathbf{q})D(\varphi)\mathrm{d}\varphi \quad (15)$$

The second order orientation factor O_s can be defined as the following equation:[7-9]

$$O_s = \int D(\varphi) \frac{(3\cos^2\varphi - 1)}{2} \, d\varphi \quad . \tag{21}$$

When $D(\varphi)$ is strongly peaked around $\varphi = 0°$ (i.e. vertical alignment), $\cos\varphi = 1$ and $O_s = 1$. On the other hand, when $\varphi = 90°$, $\cos\varphi = 0$ and $O_s = -0.5$. If the orientation is entirely random, $\langle\cos^2\varphi\rangle = 1/3$ and $O_s = 0$. Thus, O_s is a measure of the orientation of nanostructures.

REFERENCES

(1) (a) Lee, B.; Park, I.; Yoon, J.; Park, S.; Kim, J.; Kim, K.-W.; Chang, T.; Ree, M. *Macromolecules* **2005**, *38*, 4311. (b) Jin, S.; Yoon, J.; Heo, K.; Park, H.-W.; Shin, T. J.; Chang, T.; Ree, M. *J. Appl. Crystalogr.* **2007**, *40*, 950. (c) Heo, K.; Yoon, J; Jin, S.; Kim, J.; Kim, K.-W.; Shin, T. J.; Chung, B.; Chang, T.; Ree, M. *J. Appl. Cryst.* **2008**, *41*, 281. (d) Ree, M. *Macromol. Rapid Commun*. **2014**, *35*, 930.

(2) (a) Yoon, J.; Yang, S. Y.; Heo, K.; Lee, B.; Joo, W.; Kim, J. K.; Ree, M. *J. Appl. Cryst.* **2007**, *40*, 305. (b) Yoon, J.; Jin, S.; Ahn, B.; Rho, Y.; Hirai, T.; Maeda, R.; Hayakawa, T.; Kim, J.; Kim, K.-W.; Ree, M. *Macromolecules* **2008**, *41*, 8778. (c) Yoon, J.; Jung, S. Y.; Ahn, B.; Heo, K.; Jin, S.; Iyoda, T.; Yoshida, H.; Ree, M. *J. Phys. Chem. B.* **2008**, *112*, 8486.

(3) (a) Lee, B.; Park, Y.-H.; Hwang, Y.; Oh, W.; Yoon, J.; Ree, M. *Nat. Mater.* **2005**, *4*, 147. (b) Lee, B.; Oh, W.; Hwang, Y.; Park, Y.-H.; Yoon, J.; Jin, K. S.; Heo, K.; Kim, J.; Kim, K.-W.; Ree, M. *Adv. Mater*. **2005**, *17*, 696. (c) Lee, B.; Yoon, J.; Oh, W.; Hwang, Y.; Heo, K.; Jin, K. S.; Kim, J.; Kim, K.-W.; Ree, M. *Macromolecules* **2005**, *39*, 3395. (d) Lee, B.; Oh, W.; Yoon, J.; Hwang, Y.; Kim, J.; Landes, B. G.; Quintana, J. P.; Ree, M. *Macromolecules* **2005**, *38*, 8991.

(4) (a) Heo, K.; Jin, K. S.; Yoon, J.; Jin, S.; Oh, W.; Ree, M. *J. Phys. Chem. B* **2006**, *110*, 15887. (b) Heo, K.; Oh, K. S.; Yoon, J.; Jin, K. S.; Jin, S.; Choi, C. K.; Ree, M. *J. Appl. Crystallogr*. **2007**, *40*, s614. (c) Jin, K. S.; Heo, K.; Oh, W.; Yoon, J.; Lee, B.; Hwang, Y.; Kim, J.-S.; Park, Y.-H.; Chang, T.; Ree, M. *J. Appl. Crystallogr*. **2007**, *40*, s631. (d) Heo, K.; Park, S. G.; Yoon, J.; Jin, K. S.; Jin, S.; Rhee, S. W.; Ree, M. *J. Phys. Chem. C* **2007**, *111*, 10848.

(5) (a) Roe, Y. J. *Methods of X-ray and Neutron Scattering in Polymer Science*. New York: Oxford University Press; 2000. (b) Lazzari, R. *J. Appl. Crystallogr*. **2002**, *35*, 406. (c) Renaud, G.; Lazzari, R.; Leroy, F. *Surf. Sci. Rep*. **2009**, *64*, 255.

(6) (a) Pedersen, J. S. *J. Appl. Crystallogr*. **1994**, *27*, 595. (b) Hosemann, R.; Bagchi, S. N. *Direct analysis of diffraction by matter*. Amsterdam: North-Holland; 1962.

(7) (a) Yoon, J; Jin, S. K; Kim, H. C; Kim, G; Heo, K; Jin, S; Kim, J; Kim, K.-W; Ree, M. *J. Appl. Cryst*. **2007**, *40*, 476. (b) Rho, Y.; Min, J.; Yoon, J.; Ahn, B.; Jung, S.; Kim, K.; Shah, P.; Lee, J.-S.; Ree, M. *NPG Asia Mater.* **2012**, *4*, e29.

(8) (a) Ahn, B.; Kim, D. M.; Hsu, J.-C.; Ko, Y.-G.; Shin, T. J.; Kim, J.; Chen, W.-C.; Ree, M. *ACS Macro Letters* **2013**, *2*, 555. (b) Hahm, S. G.; Rho, Y.; Jung, J.; Kim, S. H.; Sajoto, T.; Kim, F. S.; Barlow, S.; Park, C. E.; Jenekhe, S. A.; Marder, S. R.; Ree, M. *Adv. Funct. Mater.* **2013**, *23*, 2060. (c) Kim, Y. Y.; Ahn, B.; Sa, S.; Jeon, M.; Roth, S. V.; Kim, S. Y.; Ree, M. *Macromolecules* **2013**, *46*, 8235. (d) Kim, K.; Kim, Y. Y.; Park, S.; Ko, Y.-G.; Rho, Y.; Kwon, W.; Shin, T. J.; Kim, J.; Ree, M. *Macromolecules* **2014**, *47*, 4397. (e) Ahn, B.; Kwon, W.; Kim, H.; Ree, M. *Polym. Chem.* **2014**, *5*, 1912.

(9) Matsuo, M.; Tamada, M.; Terada, T.; Sawatari, C.; Niwa, M. *Macromolecules* **1982**, *15*, 988.

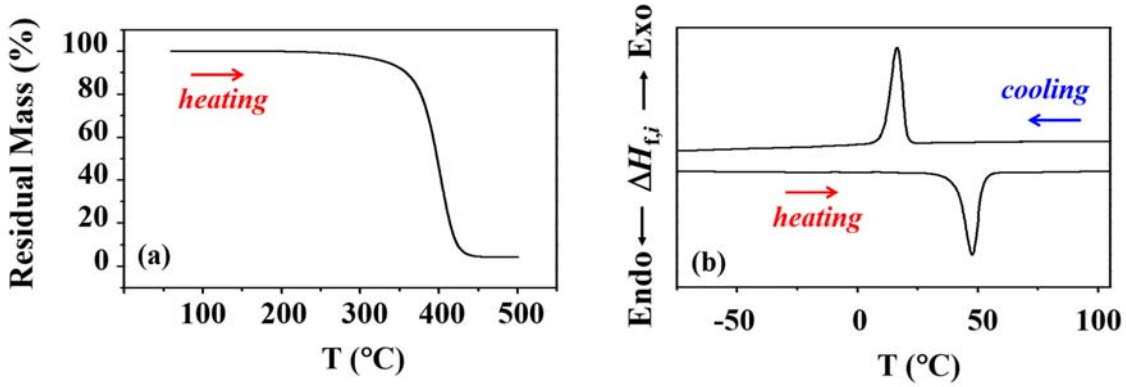

Figure S1. Thermograms of PVL homopolymer (5190 $M_{n,NMR}$; 3850 $M_{n,NMR}$ for only PVL part excluded end groups): (a) TGA thermogram; (b) DSC thermograms. All thermograms were measured at a rate of 10.0 °C min^{-1} under nitrogen atmosphere.

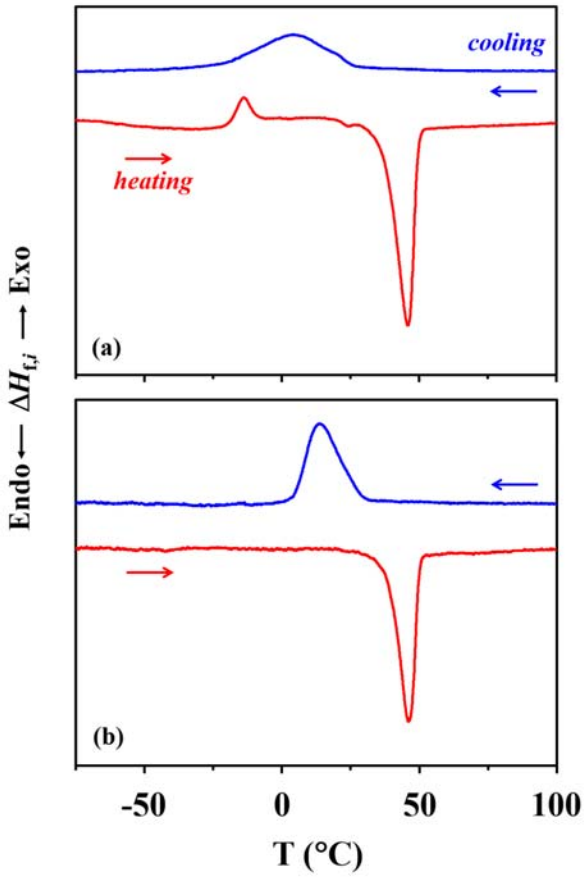

Figure S2. DSC thermograms of PVL-*b*-PS measured at two different rates: (a) 5.0 °C min^{-1}; (b) 2.0 °C min^{-1}. All measurements were conducted under nitrogen atmosphere.

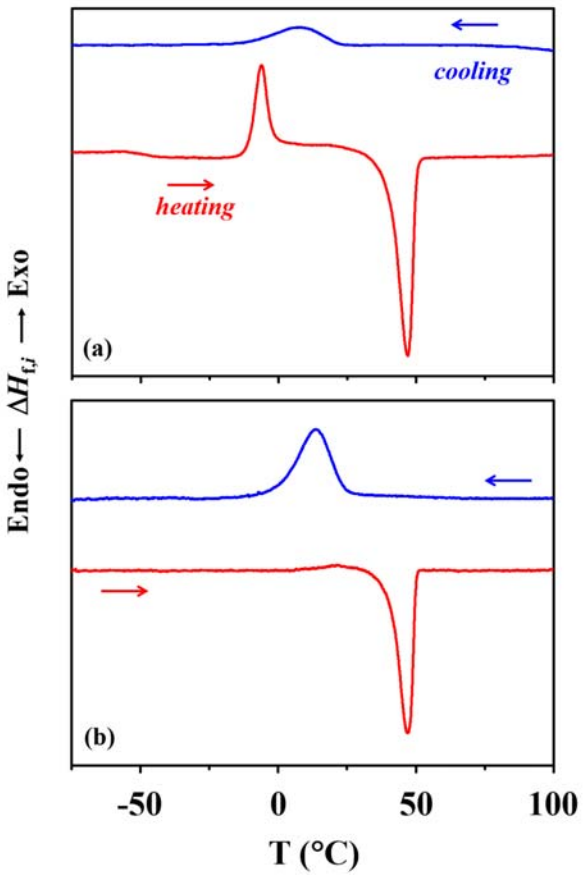

Figure S3. DSC thermograms of PVL-*rot*-PS-F measured at two different rates: (a) 5.0 °C min^{-1}; (b) 2.0 °C min^{-1}. All measurements were conducted under nitrogen atmosphere.

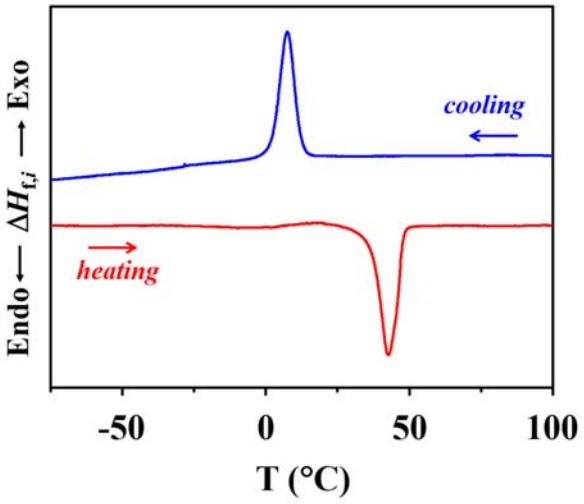

Figure S4. DSC thermograms of PVL-*rot*-PS-M measured at 5.0 °C min^{-1} under nitrogen atmosphere.

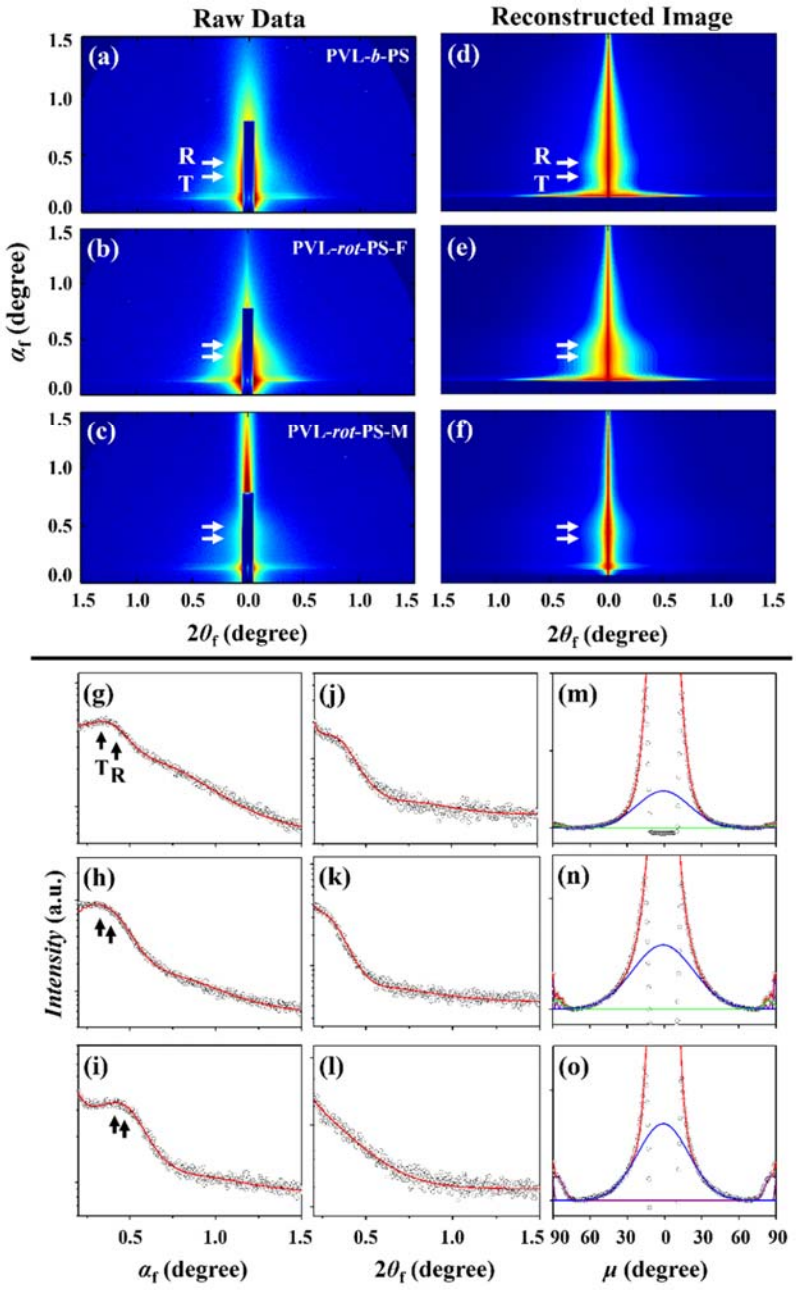

Figure S5. Representative GISAXS data of the THF-annealed films (110-130 nm thick) of PVL-*b*-PS, PVL-*rot*-PS-F, and PVL-*rot*-PS-M measured with a sample-to-detector distance (SDD) of 2910 mm using a synchrotron X-ray beam (λ = 0.12096 nm). PVL-*b*-PS: (a) 2D scattering image measured with of α_i = 0.133°; (d) 2D image reconstructed from the structural parameters in Table 3 using the GIXS formula; (g) out-of-plane scattering profile extracted along the meridian line at $2\theta_f$ = 0.123°; (j) in-plane scattering profile extracted along the equatorial line at α_f = 0.198°; (m) azimuthal scattering profile of the first-order lamellar peak at 0.371°. PVL-*rot*-PS-F: (b) 2D scattering image measured with of α_i = 0.134°; (e) 2D image reconstructed from the structural parameters in Table 3 using the GIXS formula; (h) out-of-plane scattering profile extracted along

the meridian line at $2\theta_f = 0.123°$; (k) in-plane scattering profile extracted along the equatorial line at $\alpha_f = 0.198°$; (n) azimuthal scattering profile of the first-order lamellar peak at 0.357°. PVL-*rot*-PS-M: (c) 2D scattering image measured with of $\alpha_i = 0.131°$; (f) 2D image reconstructed from the structural parameters in Table 3 using the GIXS formula; (i) out-of-plane scattering profile extracted along the meridian line at $2\theta_f = 0.107°$; (l) in-plane scattering profile extracted along the equatorial line at $\alpha_f = 0.238°$; (o) azimuthal scattering profile of the first-order lamellar peak at 0.520°. In (g–l), the symbols are the measured data and the solid lines were obtained by fitting the data using the GIXS formula of lamellar structure model. In (m–o), the symbols are the measured data and the sold lines were obtained by fitting the data using the Gaussian functions.

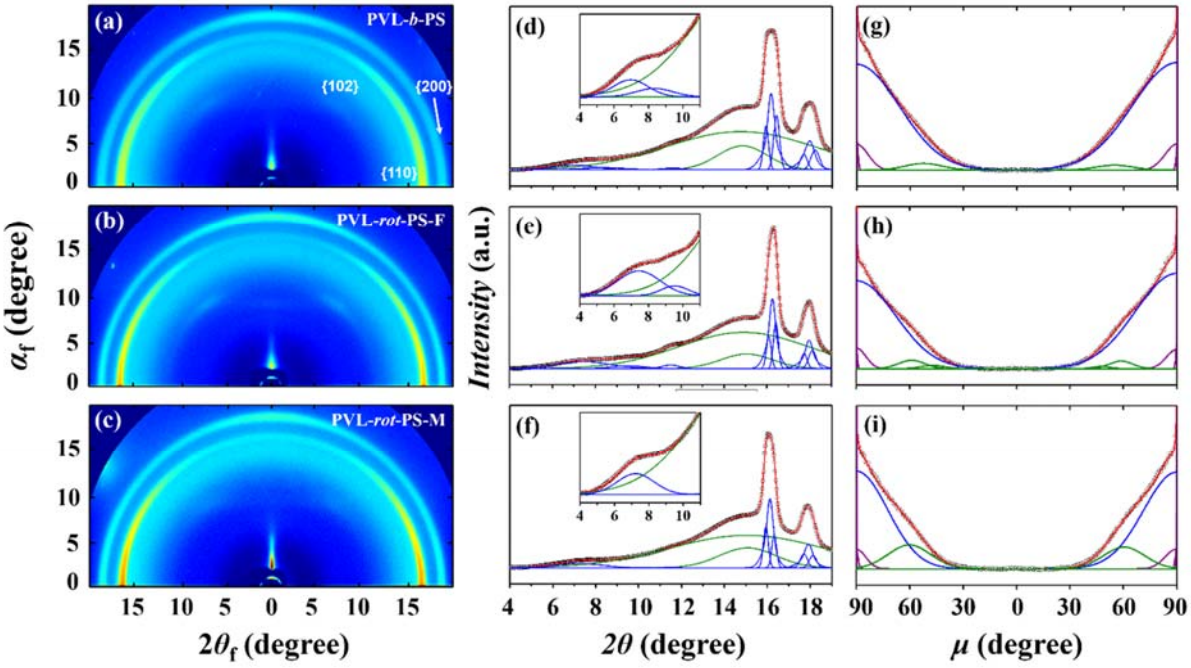

Figure S6. Representative GIWAXS patterns of the THF-annealed films (110-130 nm thick) of PVL-*b*-PS, PVL-*rot*-PS-F, and PVL-*rot*-PS-M films measured with $\alpha_i = 0.174°$ at SDD = 209 mm using a synchrotron X-ray beam ($\lambda = 0.1209$ nm). PVL-*b*-PS: (a) 2D scattering image; (d) 1D scattering profile averaged quadrantly from the 2D image in (a); (g) azimuthal scattering profile of the {110} peak. PVL-*rot*-PS-F: (b) 2D scattering image; (e) 1D scattering profile averaged quadrantly from the 2D image in (b); (h) azimuthal scattering profile of the {110} peak. PVL-*rot*-PS-M: (c) 2D scattering image; 1D scattering profile averaged quadrantly from the 2D image in (c); (i) azimuthal scattering profile of the {110} peak.

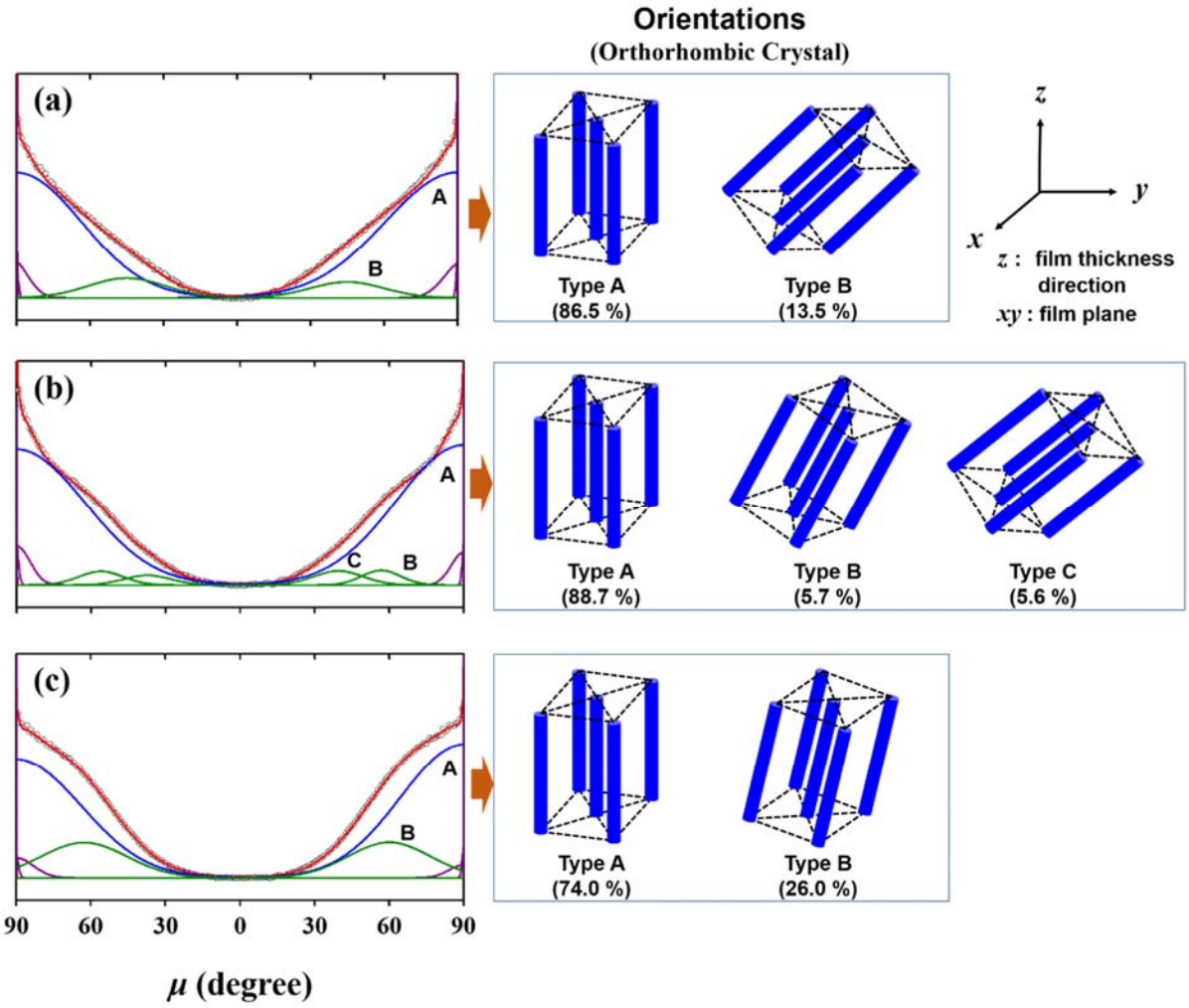

Figure S7. Azimuthal scattering profiles and analysis results of the {110} peaks of PVL crystals in Figure 5 and orientational crystal domains: (a) as-cast PVL-*b*-PS film; (b) as-cast PVL-*rot*-PS-F film; (c) as-cast PVL-*rot*-PS-M film.

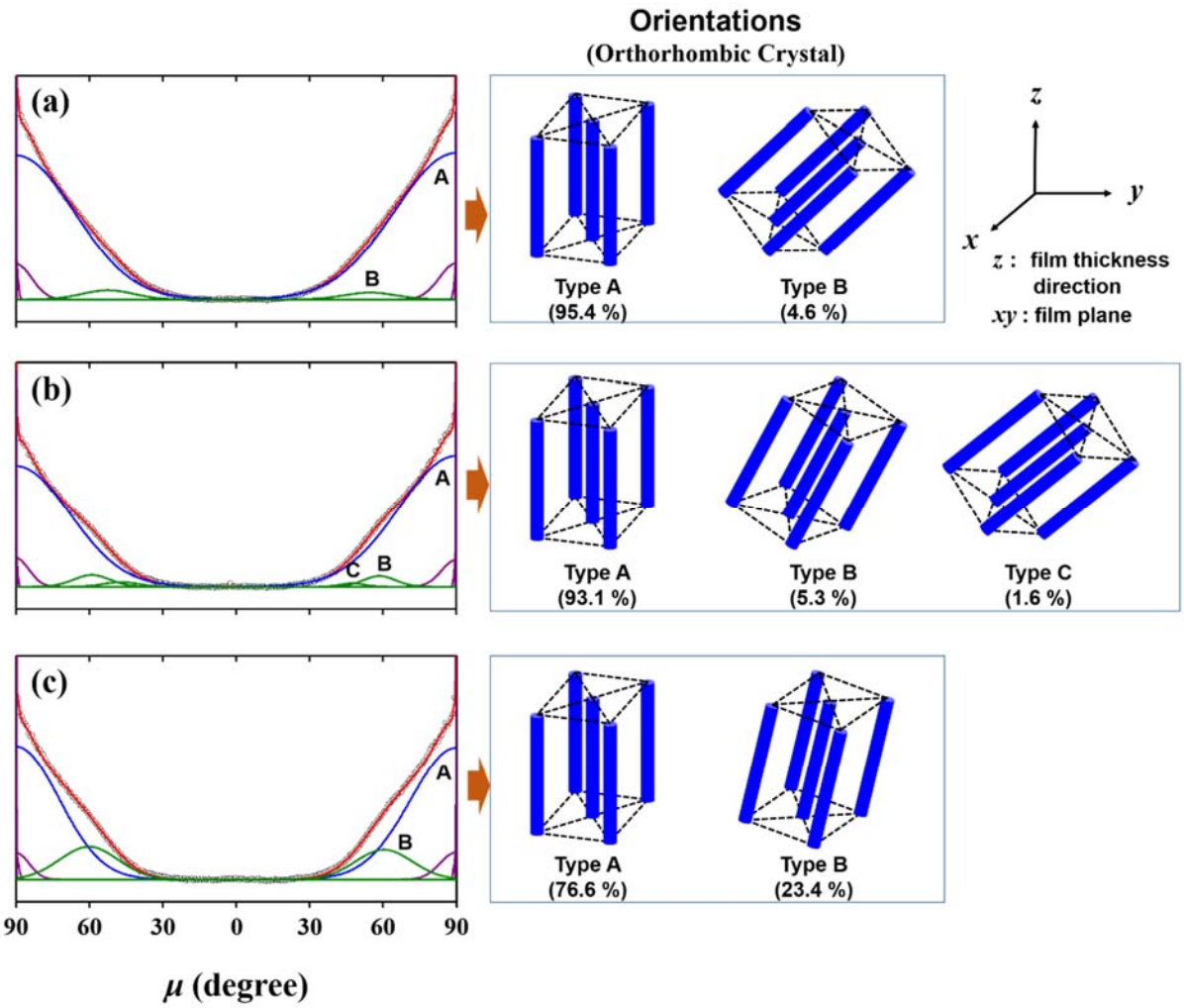

Figure S8. Azimuthal scattering profiles and analysis results of the {110} peaks of PVL crystals in Figure S6 and orientational crystal domains: (a) THF-annealed PVL-*b*-PS film; (b) THF-annealed PVL-*rot*-PS-F film; (c) THF-annealed PVL-*rot*-PS-M film.

(a)

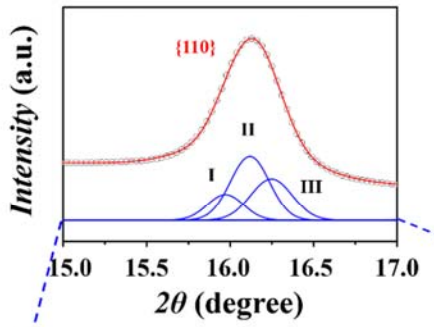

(c)

{110}	2θ (deg.)	d-spacing (nm)	ω_i (deg.)	ϕ_i (%)
I	15.973	0.435	0	18.2
II	16.119	0.431	7.8	48.4
III	16.247	0.428	10.3	33.4

(b)

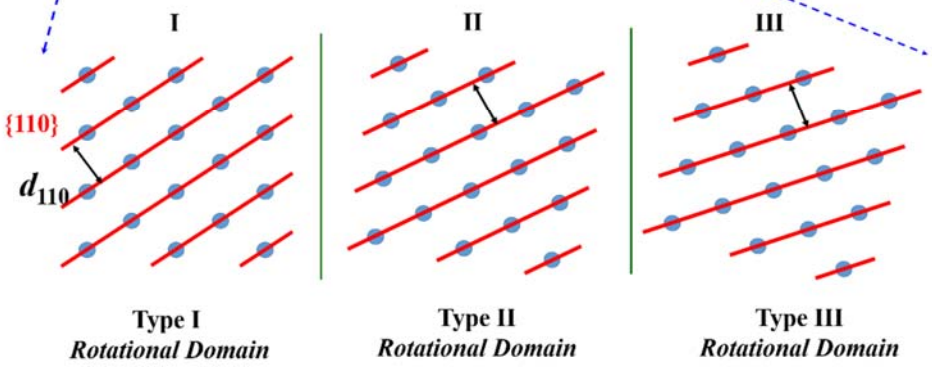

Figure S9. (a) Enlarged {110} reflection profile of PVL-*b*-PS-F film (as-cast film) obtained from the 1D scattering profile in Figure 5d. The symbols represent the measured data; the blue curves represent the scattering profiles obtained by the deconvolution of the {110} reflection profile; the red curve represents the sum of the deconvoluted scattering profiles in blue color. (b) Top views of orthorhombic lattices in three different rotational domains which were determined by the deconvolution analysis of the scattering profile in (a); d_{110} is the *d*-spacing of {110} reflection. (c) Deconvolution analysis results of the scattering profile in (a); ω_i and ϕ_i are the rotational angle and relative volume fraction of orthorhombic lattice domain *i* respectively where the rotational axis is parallel to the *c*-axis of the lattice (which is also parallel to the out-of-plane of the film).

(a)

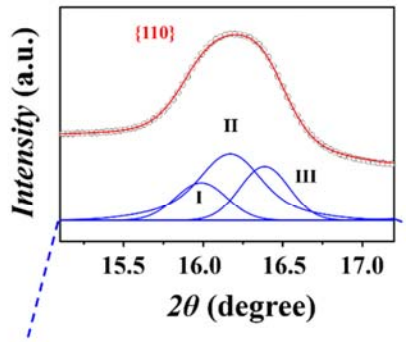

(c)

{110}	2θ (deg.)	d-spacing (nm)	ω_i (deg.)	ϕ_i (%)
I	15.985	0.435	0	20.2
II	16.167	0.430	8.7	52.0
III	16.387	0.424	12.9	27.8

(b)

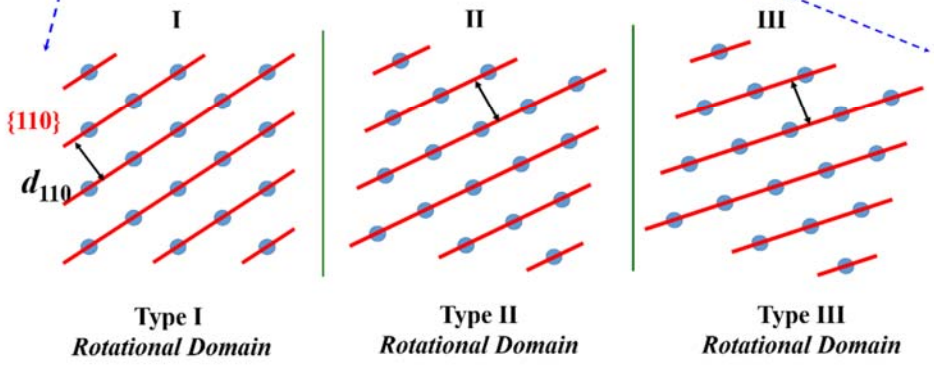

Figure S10. (a) Enlarged {110} reflection profile of PVL-*rot*-PS-F film (as-cast film) obtained from the 1D scattering profile in Figure 5e. The symbols represent the measured data; the blue curves represent the scattering profiles obtained by the deconvolution of the {110} reflection profile; the red curve represents the sum of the deconvoluted scattering profiles in blue color. (b) Top views of orthorhombic lattices in three different rotational domains which were determined by the deconvolution analysis of the scattering profile in (a); d_{110} is the *d*-spacing of {110} reflection. (c) Deconvolution analysis results of the scattering profile in (a); ω_i and ϕ_i are the rotational angle and relative volume fraction of orthorhombic lattice domain *i* respectively where the rotational axis is parallel to the *c*-axis of the lattice (which is also parallel to the out-of-plane of the film).

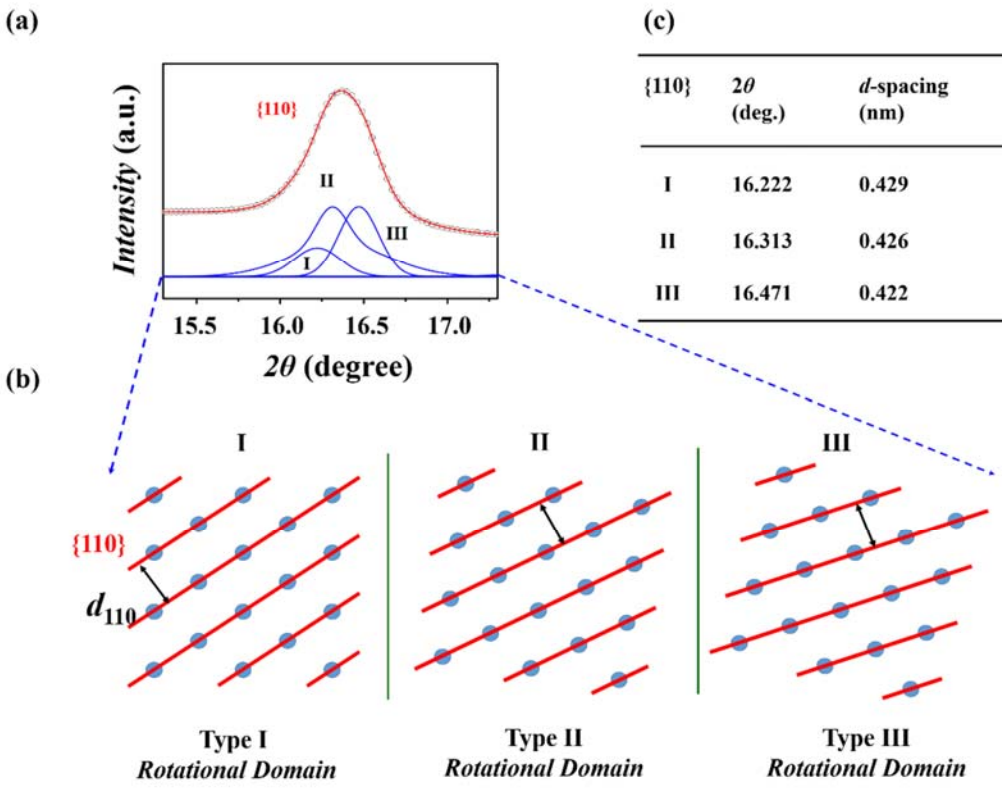

(c)

{110}	2θ (deg.)	d-spacing (nm)	ω_i (deg.)	ϕ_i (%)
I	16.222	0.429	0	15.8
II	16.313	0.426	6.8	51.3
III	16.471	0.422	10.4	32.9

Figure S11. (a) Enlarged {110} reflection profile of PVL-*rot*-PS-M film (as-cast film) obtained from the 1D scattering profile in Figure 5f. The symbols represent the measured data; the blue curves represent the scattering profiles obtained by the deconvolution of the {110} reflection profile; the red curve represents the sum of the deconvoluted scattering profiles in blue color. (b) Top views of orthorhombic lattices in three different rotational domains which were determined by the deconvolution analysis of the scattering profile in (a); d_{110} is the *d*-spacing of {110} reflection. (c) Deconvolution analysis results of the scattering profile in (a); ω_i and ϕ_i are the rotational angle and relative volume fraction of orthorhombic lattice domain *i* respectively where the rotational axis is parallel to the *c*-axis of the lattice (which is also parallel to the out-of-plane of the film).

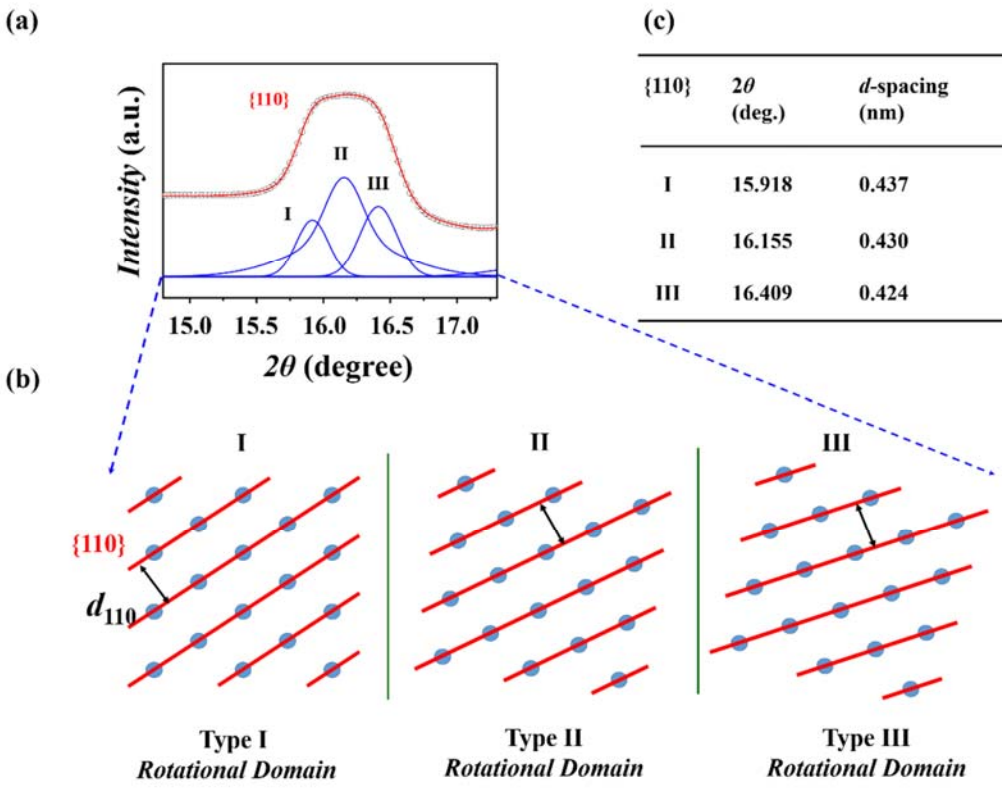

(c)

{110}	2θ (deg.)	d-spacing (nm)	ω_i (deg.)	ϕ_i (%)
I	15.918	0.437	0	17.1
II	16.155	0.430	10.3	58.7
III	16.409	0.424	14.0	24.2

Figure S12. (a) Enlarged {110} reflection profile of PVL-*b*-PS film (THF-annealed film) obtained from the 1D scattering profile in Figure S6d. The symbols represent the measured data; the blue curves represent the scattering profiles obtained by the deconvolution of the {110} reflection profile; the red curve represents the sum of the deconvoluted scattering profiles in blue color. (b) Top views of orthorhombic lattices in three different rotational domains which were determined by the deconvolution analysis of the scattering profile in (a); d_{110} is the d-spacing of {110} reflection. (c) Deconvolution analysis results of the scattering profile in (a); ω_i and ϕ_i are the rotational angle and relative volume fraction of orthorhombic lattice domain i respectively where the rotational axis is parallel to the c-axis of the lattice (which is also parallel to the out-of-plane of the film).

(a)

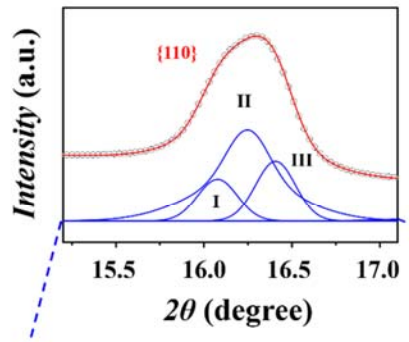

(c)

{110}	2θ (deg.)	d-spacing (nm)	ω_i (deg.)	ϕ_i (%)
I	16.078	0.432	0	16.0
II	16.247	0.428	7.8	61.2
III	16.406	0.424	11.0	22.8

(b)

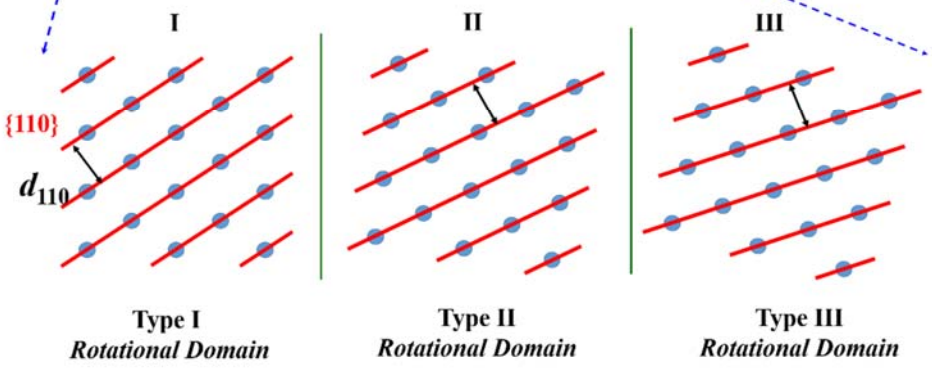

Figure S13. (a) Enlarged {110} reflection profile of PVL-*rot*-PS-F film (THF-annealed film) obtained from the 1D scattering profile in Figure S6e. The symbols represent the measured data; the blue curves represent the scattering profiles obtained by the deconvolution of the {110} reflection profile; the red curve represents the sum of the deconvoluted scattering profiles in blue color. (b) Top views of orthorhombic lattices in three different rotational domains which were determined by the deconvolution analysis of the scattering profile in (a); d_{110} is the *d*-spacing of {110} reflection. (c) Deconvolution analysis results of the scattering profile in (a); ω_i and ϕ_i are the rotational angle and relative volume fraction of orthorhombic lattice domain *i* respectively where the rotational axis is parallel to the *c*-axis of the lattice (which is also parallel to the out-of-plane of the film).

(a)

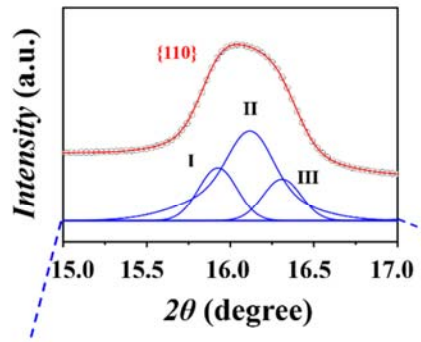

(c)

{110}	2θ (deg.)	d-spacing (nm)	ω_i (deg.)	ϕ_i (%)
I	15.925	0.437	0	21.4
II	16.118	0.431	9.5	61.8
III	16.311	0.426	12.9	16.8

(b)

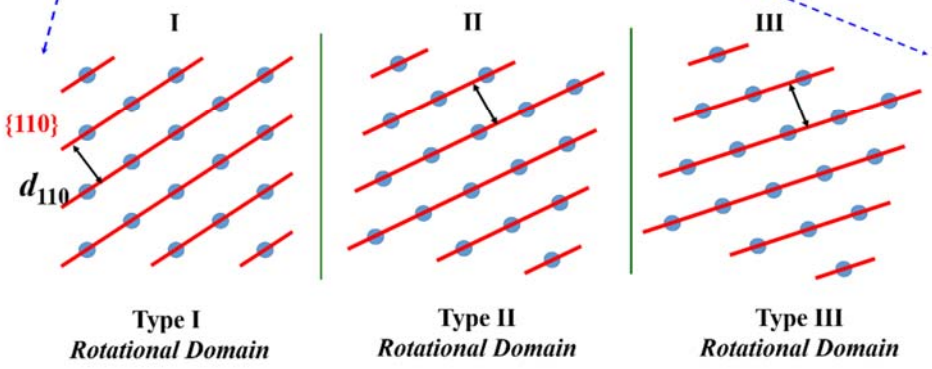

Figure S14. (a) Enlarged {110} reflection profile of PVL-*rot*-PS-M film (THF-annealed film) obtained from the 1D scattering profile in Figure S6f. The symbols represent the measured data; the blue curves represent the scattering profiles obtained by the deconvolution of the {110} reflection profile; the red curve represents the sum of the deconvoluted scattering profiles in blue color. (b) Top views of orthorhombic lattices in three different rotational domains which were determined by the deconvolution analysis of the scattering profile in (a); d_{110} is the *d*-spacing of {110} reflection. (c) Deconvolution analysis results of the scattering profile in (a); ω_i and ϕ_i are the rotational angle and relative volume fraction of orthorhombic lattice domain *i* respectively where the rotational axis is parallel to the *c*-axis of the lattice (which is also parallel to the out-of-plane of the film).

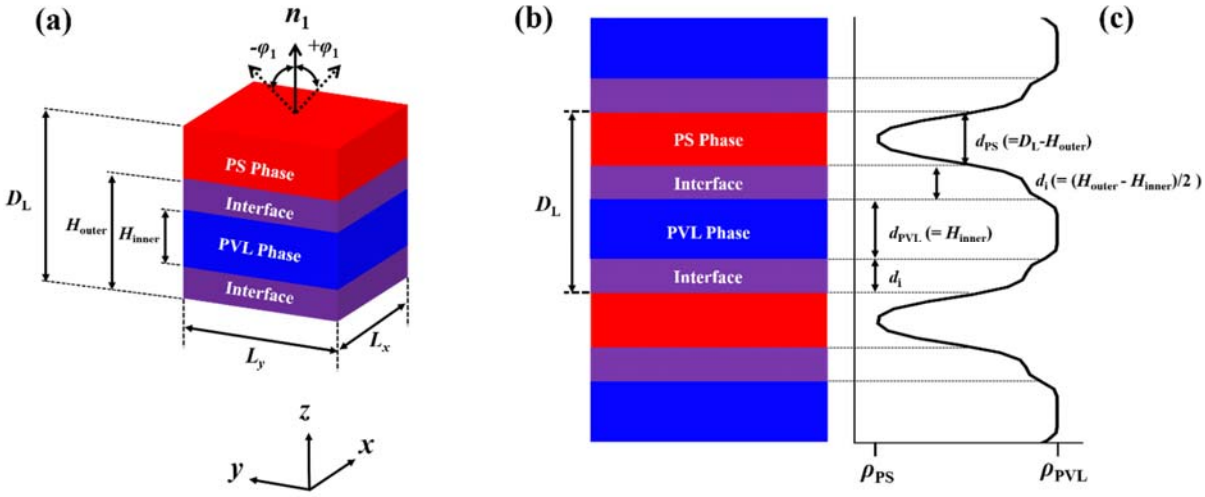

Figure S15. A lamellar structure model composed of three layers: (a) 3D representation of lamellar structure where $\boldsymbol{n_1}$ is the orientation vector of the structure and φ_1 is the polar angle between the $\boldsymbol{n_1}$ vector and the out-of-plane of the film; (b) 2D representation of lamellar structure. The inner and outer layers in (a) correspond to the dense and interfacial layers in (b) respectively; the blue colored layer in (b) corresponds to the less dense layer; (c) The electron density profile along the direction of layer stacks in the lamellar structure where ρ_{PVL} and ρ_{PS} are the electron densities of crystalline (dense) and amorphous (less dense) layers respectively. The dimension of the lamellar structure is defined by D_L (long period), L_x, L_y, d_{PVL} (= H_{inner}), d_i (= (H_{outer} – H_{inner})/2), and d_{PS} (= D_L – H_{outer}).